CALCULATION OF CONSTITUENT POROSITY IN A DUAL-POROSITY MATRIX: MRI AND IMAGE ANALYSIS INTEGRATION

Daniela Mattiello, Massimo Balzarini, Lamberto Ferraccioli, Alberto Brancolini

AGIP SpA

Abstract

Fracture and vug porosity and permeability measurement still remain an open problem for core analysis labs. These data are of primary importance, mainly in carbonate reservoirs, for a correct simulation of the field performance in terms of stored hydrocarbon volume, fluid dynamics and matrix/fracture exchange. Conventional image analysis on core by scanning electron microscope (SEM) on thin sections does not retain the complete 3D information. Use of non-destructive imaging techniques such as CT X-ray and Magnetic Resonance Imaging (MRI) seems to be the more interesting approach to the problem. In this paper we present a proprietary software tool which allows the interactive processing and interpretation of 2D and 3D MRI of core.

Currently MRI data are used in laboratory analysis, mainly for semi-quantitative description of core samples. We will highlight that MRI core data can be better and more cost effectively exploited if numerical processing and analysis are applied to gather quantitative information about petrophysical properties, namely porosity and permeability.

We will present how numerical core analysis can be performed on 2D MRI data, by means of a software tool which is based on computerized image analysis and processing techniques. In particular, this tool can significantly contribute to the quantitative analysis of MRI data for calculating constituent porosity in a dual porosity matrix. Moreover, innovative modeling techniques are incorporated in the tool, in order to automatically segment core images, to separate different porosity contributions (vugs, fractures, microporosity or other).

We will then show how these techniques can be directly applied to 3D MRI core data and discuss a case study.

Introduction

Fracture and vug porosity and permeability are of great importance because of their relevance on stored hydrocarbon volume, fluid dynamics and matrix-fracture exchanges - especially in carbonate reservoirs. In these reservoirs porosity can be divided into two main types: primary (depositional) and secondary (diagenetic-tectonic) (Ref. 1).

Many papers are dedicated to the problem of discriminating between matrix and fracture porosity and, more generally, to the recognition of different pore types and their relative contributions to the total porosity (Ref. 2). At present, conventional core analysis porosity

measurements are able to quantify the total value of the parameter but fail when they try to discriminate the single contribution of a pore class. Nevertheless, we can define a pore type as a class of porosity characterized by a unique geometry (size, shape, distribution and frequency). The understanding of the nature and distribution of pore types is important especially with decreasing porosity values. In such rocks, in fact, reservoir behavior is less dependent on total porosity than on the pore type distribution (Ref. 2). Classical methods used to investigate the different porosity components are based on image analysis. The quantification is carried out on 2-dimensional images using thin sections and SEM, but there are problems related with the destructive nature of these sampling methods and the extension of two-dimensional data to three dimensions (Ref. 3).

Non destructive imaging techniques such as CT X-ray and MRI are routinely used to obtain images of the rock samples along any arbitrary plane and can be used to derive quantitative information on the fluid content. At the same time, structures such as vugs, fractures and different pore types can be qualitatively recognized by the human eye from these images. While the CT technique is mainly based on the analysis of porosity histograms to distinguish the contribution of the pore volume from the fractures (Ref. 4), in this paper we will present an approach based on automatic image analysis, processing and segmentation, showing that more sophisticated methods can be used to separate different pore classes. In particular, in our method, the images we started with were obtained by Nuclear Magnetic Resonance (NMR) imaging which gives the spatial fluid saturation inside the rock. Generally these measurements are influenced not only by the porosity structures, but also by parameters such as pore volume, surface-to-volume ratio (S/V), fluid content and composition which yield a final complex product. Therefore, if on the one hand NMR images are easily obtained, at least for limestone samples, on the other it is always necessary to process the images before any computation for deriving quantitative and complete classification of the pore structures can be carried out. Since the image processing techniques best suited to this problem are, in general, difficult to choose, and their fine tuning is beyond the scope of a petrographer, we chose to build a software tool to assist him/her while analyzing, discriminating, classifying and calculating porosity on core samples images. The software we developed can automatically discriminate different pore classes, grouping them into porosity types and characterizing each item by volume, sharpness, heterogeneity. The petrographer can then group one or more of the classes, using his/her experience, and then calculate the respective porosity values inside each slice.

Imaging Techniques

NMR is radiofrequency spectroscopy based on the excitation of nuclear energy levels, mainly in hydrogen nuclei, split by means of an external static field B_0 (2.4 T, in the spectrometer we used). The return to equilibrium, after turning off the RF, generates a signal proportional to the fluid content and whose decay is characterized by two different times: the spin-lattice relaxation time, T1, and the spin-spin relaxation time, T2 (Ref. 5). The basic NMR physical phenomena, just described, can be applied in different ways for extracting a wide spectrum of information on the fluids that saturate a rock sample. For example, MRI is a tomographic technique which uses a magnetic field gradient to encode

signal coming from different sample parts, guaranteeing spatially resolved images. A series of gradients correctly oriented in 3D space generates a spatially dependent distribution of MRI frequencies that can be computer processed to obtain an image of the rock fluids distribution that is also a function of the pore system. In addition, the solid matrix does not interfere with measurements of fluids, whose properties, such as relaxation times, diffusion coefficient and chemical composition can be measured. As previously mentioned, the MRI signal is proportional to the number of nuclei present in the analyzed region, and it is upon this effect that the method for computing porosity using MRI is based. In particular, a mass reference was used to convert the experimental MRI signal amplitudes into porosity. This reference has the same proton density as the fluid in the rock, so the conversion was performed considering the porosity in the reference as 100%. Specifically, the following formula was applied for each pixel in the core image, where M is the magnetization and V the pixel volume:

$$\Phi_{core} = \Phi_{ref} * \frac{V_{ref} M_{core}}{V_{core} M_{ref}} \quad \text{..... (1)}$$

The MRI porosity measurement can be considered as a direct measurement. Because the acquired magnetization is reduced by the relaxation process, in order to calculate the total porosity, an accurate fitting of the MRI experimental data is necessary to obtain the initial magnetization value M_0 and $T_{1,2}$.

Another important feature of MRI to point out is that the images are characterized by a signal which is not only proportional to the fluid content, but also to the relaxation time (T_2 in our experiment) which is an indicator of the confining geometry. In our experiments we measured the hydrogen density map using MRI sequence based on the CPMG (Ref. 5), on transverse sections. In this way the structures could be characterized both for their “shape” and for their T_2 behavior. In particular large pores will exhibit higher T_2 values with respect to small ones: for this reason MRI can discriminate directly pore dimensions.

All these mentioned features make MRI techniques useful for examining core samples. In particular it is a non destructive technique and multiple experiments, such as fluid flow through samples, may be conducted with the same, single rock sample.

Manual vs. Automatic Image Analysis

We will now describe the image processing methods we used to analyze the NMR core images, and to obtain the constituent porosity. We define as constituent porosity all contributions associated to specific features such as fractures or vugs (Ref. 6). More details on the processing techniques we used can be found in references 9 to 13, since they are beyond the scope of the present paper.

Figures 1 and 2 present the intensity maps (in false colors) relative to two core samples slices. The relevant features of vugs and fractures can either be detected by visual inspection and selection of zones on the images, or by thresholding them. Both methods suffer from lack of objectivity and repeatability. For instance, the human eye can immediately detect isolated vugs, fractures and other porosity classes, but the classification is not unique, since

another expert could (almost certainly) point out different relevant features. It is also well known that the human eye can easily detect lines, even when they do not exist (Ref. 7). The effects of choosing a different value for thresholding are shown in figures 3. By thresholding one selects only the image zones where the signal intensity is above the selected threshold, so that the resulting image can be used as a mask for computing porosity. Using the masks in figures 3b and 3c, where the thresholds are respectively 16 % and 21% of the maximum intensity, the values for partial porosity are respectively 4.22% and 2.74%. Note that the two thresholds differ by 5% while the resulting porosity difference is about 50%. Other problems are due to low image resolution and noise, which can significantly alter the visual interpretation.

Is it possible to establish an objective and repeatable criterion to classify different porosity types? The solution we propose is built upon an automatic method of classification of the image zones on NMR images which guarantees the requested objectivity and repeatability. The human expertise is the key factor in the following selection phase, which is in turn based on the results of the previous, automatic steps. The correct mix of the automatic and expert results can thus be achieved.

NMR Image Processing

Our method is based on the assumption that there exists an underlying statistical model that describes the spatial and physical interaction between adjacent pixels. This implies that neighboring pixels can be grouped into a single class if they belong to the same statistical population. So a simplified image, or mask, can be computed from the intensity image, by assigning each pixel to a class. The user chooses the number of classes after a visual inspection of the sample slices: our experiments show that a reasonable value usually is near, or in the order of the different constituents number. This descends from the final goal, namely to detect porosity mainly coming from vugs and fractures, discarding other contributions. The algorithms can also model the inter-regional spatial relations, thus better describing the complex interactions that can occur inside the sample. The user chooses the parameters of the statistical model in order to get a faithful representation of the image, in terms of correlation between adjacent pixels. Once the mask image is generated by the classification algorithms, the user can compute the porosity due to a constituent by selecting that single class on the mask. We tried several classification algorithms, and found the best results using a combination of statistical and probabilistic approaches. Figure 4a shows an original intensity image, and the corresponding classification results are shown in figure 4b: note that the image has been significantly simplified, while retaining all the relevant features. Figure 4c shows the mask obtained by selecting class 4, which is represented by the green color. This mask can be used to compute the porosity due to the selected constituents.

Pixels belonging to the same class can further be classified as belonging to the same shape, if they are connected. So, the user can also build a mask formed by single shapes and/or single classes. Figures 5a and 5b show respectively the intensity map and the mask obtained by selecting the class of the fracture and shapes whose area is above a defined threshold, which presumably correspond to an isolated vug and large zones of significant porosity.

Experiments

A series of MRI measurements on 9 water saturated core plugs (2'' diameter and 3'' length) were performed. The rock samples were representative of a fractured dolomite reservoir where the diagenetic evolution created both small intercrystalline pores and large dissolution vugs. The samples were twice Soxlhet extracted, first using toluene and then using methyl alcohol. Conventional porosity measurements were determined by the water saturation method. In this study a multi-slice multi-echo (**MSME**) sequence, based on the CPMG method, was used (Ref. 5). A series of echoes is generated by the repeated application of selective 180° pulses. A key factor in this kind of experiment is the constant echo time (TE), which must be kept as low as possible. An optimal value for TE is the result of a compromise between the size of the acquisition matrix and the resolution of the image. In our acquisitions the value of TE was 4.8 ms and no diffusion effects were noticeable. The multi-echo acquisition was then fitted pixel-by-pixel according to the following equation:

$$M(t) = M_0 e^{-t/T_2} \quad \text{.....(2)}$$

and the intrinsic magnetization M_0 and the T_2 time determined. The porosity was then calculated by comparison with the reference sample using formula (1). This simple mono-exponential behavior was assumed because of the relatively long typical relaxation time of this lithology , although more complex fittings could be used in other situations (Ref. 8). For each sample, eight transversal slices were acquired with 5 mm slice thickness and 5 mm interslice distance. The acquisition scheme is shown in figure 6.

Total porosity was determined from image analysis and compared with that measured by conventional laboratory methods. For two samples the contribution from vugs and fractures was compared to the SEM technique. The NMR total porosity was computed using equation 1, that is taking into account all pixels that show non-null intensity. The NMR secondary porosity was calculated first by classifying each zone on the NMR fitted images, as explained in the previous paragraphs, then by selecting all the zones that, according to the petrographer's interpretation, correspond either to fractures or to vugs. The software we developed lets the user select such zones interactively and directly on each image. So the petrographer can either select one or more classes and use them as masks for the computation of the corresponding porosity, or go further with image processing using geometrical and shape characteristics of each region. Using logical operators the petrographer can extract from one or more classes the shapes that best suit his/her visual interpretation of the core images. The combination of logical operators is achieved in a visual programming environment, with "drag and drop" of the corresponding icons and their mouse linking, as appropriate.

Discussion

The following table shows the measured total porosity values, compared with those calculated on the MSME images and on SEM images for two cores. The two last columns show the computed constituent porosity, both on MRI images and on SEM images.

SAMPLE	PERMEABILITY (mD)		LAB POROSITY	NMR TOTAL POROSITY	SEM TOTAL POROSITY	NMR CONSTITUENT POROSITY	SEM CONSTITUENT POROSITY
	HORIZ.	VERT.	%	%	%	%	%
49	159	1.05	3.6	4.58		1.56	
67	3.54	0.06	5.2	7.11		1.58	
310	15.04	5.03	4.1	3.07		1.30	
313	0.65	1452	3.9	3.81		0.65	
319	503	4.05	8.7	8.67	6.34	2.4	1.32 (*)
337	1400	279	3.6	3.29		0.84	
499	10.3	12.2	3.5	2.60		0.39	
460	30.1	16.6	6.7	5.05		3.25	
463	39.6	10.2	6	4.53	4.93	1.58	2.09 (*)

TABLE 1. Petrophysical measured and computed parameters. (*) SEM secondary porosity takes into account fractures and vugs with $\varnothing > 1$ mm.

In order to explain total porosity differences in Table 1 we have to point out some peculiarities of each method.

First of all, the examined samples are very heterogeneous, as highlighted by comparing the difference between vertical and horizontal permeabilities (cols. 2 and 3). The MSME technique imaged only half of the core sample, thus explaining some of the difference.

Secondly, conventional porosity measurements assume that the considered volume is composed of a perfect cylinder. Surface structures, being water saturated, contribute to the total porosity. MRI measurements, on the other hand, are performed after removing the water surface, to reduce image artifacts. The SEM results on the two selected samples were obtained excluding the outer part of the sample, leading to comparable values.

Another point to be stressed is that MRI techniques have to be applied in a carefully controlled environment, because small differences in experimental conditions give rise to different results. So the correct sample excitation, field homogeneity, and sample heterogeneity are factors that could explain the experimental differences.

On the image processing side of the proposed method, we must point out that background noise can significantly alter the overall results. We found that it can significantly vary and can sum up to 9% of the useful signal under particular sampling conditions. As already said, the segmenting and classifying algorithms take into account the background noise, but it nevertheless can significantly disturb the final result.

After pointing out the well known problems, we want to stress some advantages of the proposed method.

By comparison with the results obtained by SEM, the calculated total and constituent porosity values are in good agreement. SEM results shown in table 1 take into account fractures and pores with diameter > 1 mm, which is the resolution of the images used for calculations. Table 2 shows the comparison between overall SEM results and the values

computed on the NMR images when taking into account features with comparable resolution (≈ 1 mm).

SAMPLE 319			
SEM features	**Porosity value**	**MRI Chosen parameters**	**Porosity value**
fractures	0.63 %	1 class selection	0.56 %
pores ∅ > 1000 μ	0.69 %	1 class selection + shapes selected by area and sides ratio values	1.80 %
pores 50μ<∅<1000μ	4.23 %		
pores ∅ < 50 μ	0.79 %		

TABLE 2. Comparison between SEM and NMR results.

An advantage of the proposed method lies in its objectivity and repeatability, as already stressed. The method is also computer intensive, but obviously much less costly than the petrographer's time necessary to visually threshold the images in order to select the proper zones on the image.

Using MRI we can obtain maps of relevant parameters, such as relaxation time T_2, which are strong pointers of the confining geometry and that can be used for discriminating different constituents. Figure 7b shows the T_2 map relative to the intensity map in figure 7a, and clearly shows longest T_2 times for the fracture.

Finally, the method can immediately be extended to 3D NMR data. Our preliminary experiments show quite good results, especially on fractured samples, since MRI can reconstruct very carefully the fracture pattern. In one case, the calculated results are in very good accordance with fracture measures taken on core high resolution photographs.

Conclusions

In this paper we have shown that it is possible to calculate the core constituent porosities using MRI. The main advantage is that the technique is fast and non destructive, and takes advantage of the software environment we built. In addition to the porosity information, which can also be obtained by other non destructive methods such as X-ray tomography, MRI relaxation time T_2 gives information about the confining geometries and their dimension, which cannot otherwise be derived. This information can be directly used or further processed, to obtain the desired porosity classes.

The proposed image processing techniques can significantly help in reducing the overall calculation times and enhance objectiveness and repeatability.

We found good agreement between MRI and SEM for pore structures with dimension of 1 mm.

Acknowledgments

We wish to thank AGIP management for permission to publish this paper and numerous AGIP personnel for assistance with this work.

References

1. Tucker M.E., *Sedimentary petrology*, Blackwell Scientific Publications, UK, 1991, p 154

2. Davies D.K., "Image Analysis of reservoir pore systems: state of the art in solving problems related to reservoir quality", SPE 19407, 1990

3. Coles M.E., Spanne P., Muegge E.L., Jones K.W., "Computed microtomography of reservoir core samples", SCA-9401, 1994

4. Pepin G.P., "Quantitative CT core analysis for reservoir characterization", International Symposium of the Society of Core Analysts, CT Workshop, 1994

5. Callaghan P.T., *Principles of nuclear magnetic resonance spectroscopy*, Oxford Science Publications, UK, 1991

6. Moss R.P.M., Pepin G.P., Davis L.A., "Direct measurement of the constituent porosity in a dual porosity matrix", Log Analysist, March-April 1992, pp. 126-135

7. Baker V.R., *The channels of Mars*, University of Texas Press, Austin, 1982

8. Brancolini A., Cominelli A., Kulkarni R., Watson A.T, "Spatial distribution of petrophysical parameters on a core scale using Magnetic Resonance Imaging", to be presented at the 38th Annual Symposium, Society of Professional Well Log Analysts, June 1997, Houston, Texas

9. Zamperoni P., *Metodi dell'elaborazione digitale di immagini*, Masson, Milano, Italy, 1990, pp. 15-36, 71-88, 134-144

10. Gonzalez R.C., Woods R.E., *Digital Image Processing*, Addison-Wesley Publishing Company, Reading, Mass., 1992, pp. 413-465

11. Jain A.K., *Fundamentals of Digital Image Processing*, Prentice Hall, Englewood Cliffs, NJ, 1989, pp. 233-244, 362-394

12. Chou P.B. Brown C.M., "The theory and practice of Bayesian image labelling", International Journal of Computer Vision, 1990, **(4),** pp. 185-210

13. Geman S. Geman D., "Stochastic relaxation, Gibbs distributions and the Bayesian restoration of images", IEEE Transactions on Pattern Analysis and Machine Intelligence, 1984, (6) 6, pp. 721-741

Figures

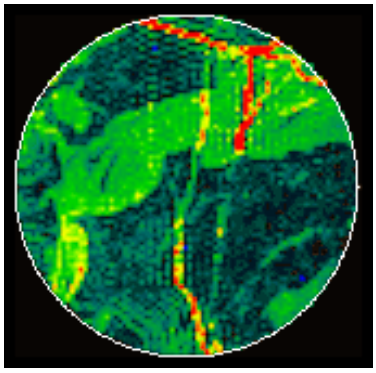

Figure 1. Intensity map in false colors (slice 1)

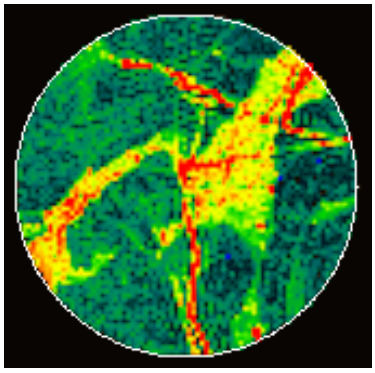

Figure 2. Intensity map in false colors (slice 2)

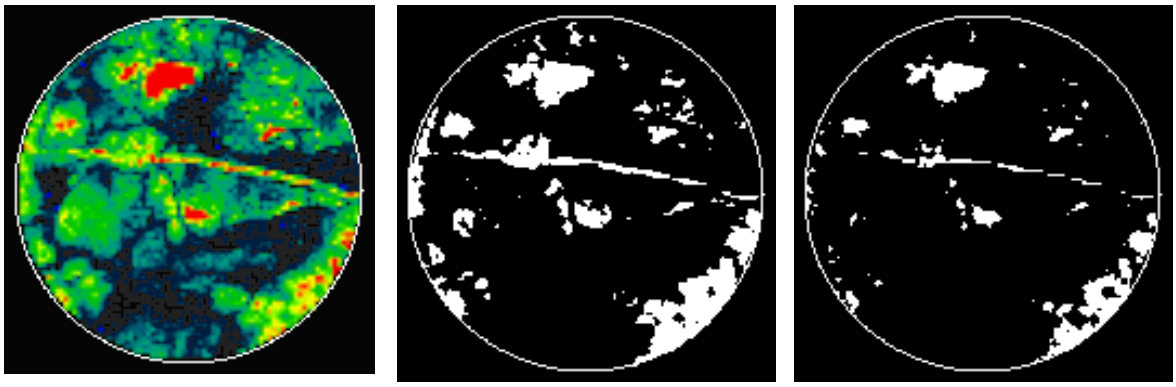

Figure 3a Figure 3b Figure 3c

Figure 3. Slice 3: intensity map in false colors (fig. 3a), and the effects of different threshold levels: threshold=0.16*$M_{0\ max}$ gives Φ = 4.22 (figure 3b), threshold=0.21*$M_{0\ max}$ gives Φ = 2.74 (fig. 3c)

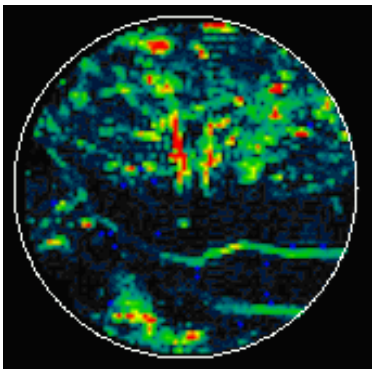

Figure 4a . Slice 4: Intensity map in false colors

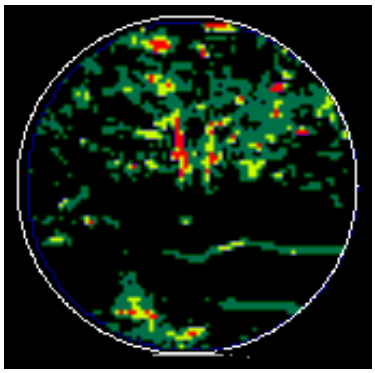

Figure 4b: Slice 4: the classification results

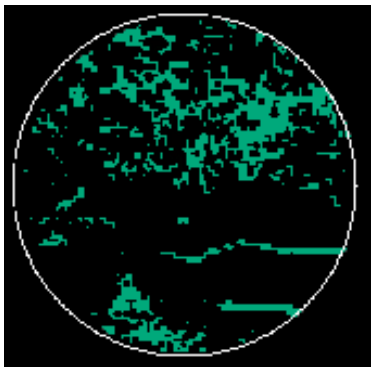

Figure 4c: Slice 4: selection of a single class

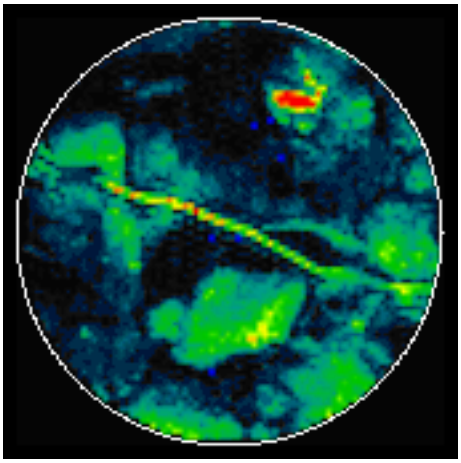

Figure 5a. Slice 5: the intensity map in false colors

Figure 5b. Slice 5: the mask for computing the constituent porosity

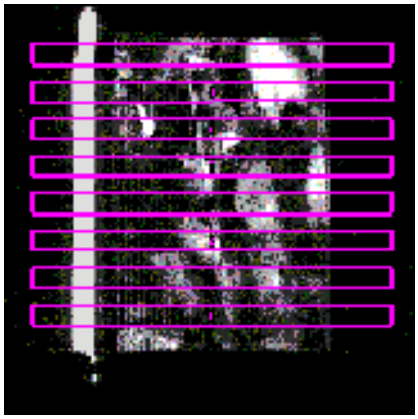

Figure 6. The acquisition frame

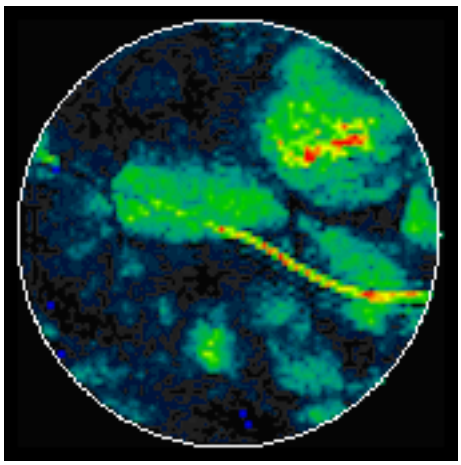

Figure 7a. Slice 6: the intensity map in false colors

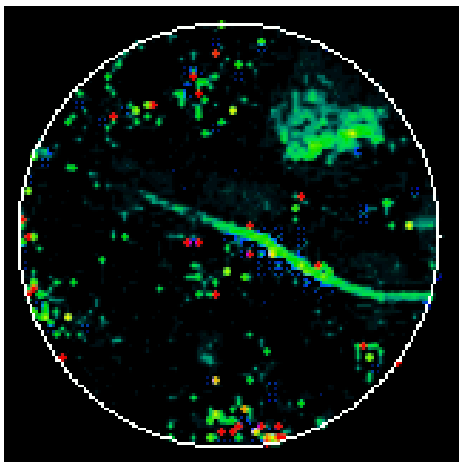

Figure 7b. Slice 6: the T_2 map